Heliyon 11 (2025) e38835

Contents lists available at ScienceDirect

Heliyon

journal homepage: www.cell.com/heliyon

Research article

Long noncoding RNA Gm4419 promotes mesangial cell proliferation and extracellular matrix accumulation *via* the miR-455-3p/histone deacetylase 2 axis

Yang Wen, Hua Gan, Qing Zhong, Ying Gong *

Department of Nephrology, The First Affiliated Hospital of Chongqing Medical University, Chongqing, 400016, China

ARTICLE INFO

Keywords:
Diabetic nephropathy
Extracellular matrix
Gm4419
miR-455-3p
Histone deacetylase 2

ABSTRACT

Long noncoding RNAs may function as competitive endogenous RNAs by sponging microRNAs, thereby contributing to the progression of diabetic nephropathy. In this study, a potential diabetic nephropathy-related long noncoding-microRNA-mRNA axis, Gm4419-miR-455-3p-*Hdac2*, was predicted using bioinformatics methods. To verify the role of the Gm4419-miR-455-3p-*Hdac2* axis in diabetic nephropathy, an *in vitro* high glucose-induced mesangial cell model was established. The expression levels of Gm4419, miR-455-3p and *Hdac2* were detected using reverse-transcription quantitative PCR. Protein levels of collagen IV, fibronectin and transforming growth factor-beta 1 were detected using western blotting. Cell counting kit-8 assay and 5-ethynyl-2′-deoxyuridine staining assay were adopted to assess cell proliferation. Cell transfection, fluorescence in situ hybridization, RNA immunoprecipitation, and dual luciferase reporter assay were also performed. Our results revealed significant cell proliferation and extracellular matrix accumulation in high glucose-treated mesangial cells. In addition, Gm4419 and *Hdac2* levels were increased and miR-455-3p was decreased in high glucose-treated mesangial cells. The interaction between Gm4419 and miR-455-3p or miR-455-3p and *Hdac2* was confirmed by reverse-transcription quantitative PCR and dual luciferase reporter assay. Gene silencing of Gm4419 inhibited mesangial cells proliferation and extracellular matrix accumulation. MiR-455-3p inhibitor counteracted the effects of Gm4419 gene silencing on cell proliferation and extracellular matrix accumulation, which was reversed again by *Hdac2* gene silencing. In summary, our research indicates that gene silencing of Gm4419 can effectively inhibit high glucose-induced mesangial cells proliferation and extracellular matrix accumulation. This is achieved through the regulation of the miR-455-3p/*Hdac2* axis, highlighting the potential of the Gm4419-miR-455-3p-*Hdac2* axis as a promising therapeutic target for the treatment of diabetic nephropathy.

1. Introduction

Diabetic nephropathy (DN) is a serious complication of diabetes mellitus that can progress to end-stage kidney failure. Despite significant advancements in the diagnosis and treatment of DN in recent years, there is still a need for more effective strategies to manage this disease. High glucose (HG)-induced dysfunction of glomerular mesangial cells has been found to be involved in the

* Corresponding author. Department of Nephrology, The First Affiliated Hospital of Chongqing Medical University, No.1 Youyi Road, Yuanjiagang, Yuzhong District, Chongqing 400016, China.
E-mail addresses: wysxm1990@126.com (Y. Wen), gong923@163.com (Y. Gong).

https://doi.org/10.1016/j.heliyon.2024.e38835
Received 14 June 2023; Received in revised form 15 September 2024; Accepted 1 October 2024
Available online 2 October 2024

development and progression of DN [1]; therefore, *in vitro* models of HG-induced mesangial cells injury are often employed to investigate the pathogenesis of DN and develop effective strategies for this troublesome condition [2–4].

Recently, long noncoding RNAs (lncRNAs) have garnered significant attention due to their potential in the diagnosis, prognosis and treatment of DN [5]. In addition, lncRNAs may function as competitive endogenous RNAs (ceRNAs) by sponging microRNAs (miRNAs), thereby contributing to the progression of DN. For instance, Li et al. reported that lncRNA potassium voltage-gated channel subfamily Q member 1 overlapping transcript 1 (KCNQ1OT1) promotes HG-induced cell proliferation, oxidative stress, and extracellular matrix accumulation in mesangial cells by sponging miR-18b [4]. Similarly, Zhang et al. found that lncRNA cancer susceptibility candidate 2 (CASC2) is down-regulated in DN serum and HG-induced human mesangial cells, and upregulation of CASC2 inhibits HG-induced mesangial cells proliferation, oxidative stress and extracellular matrix accumulation *via* the miR-133b/forkhead box P1 (*FOXP1*) axis [6]. Numerous other lncRNA-miRNA-mRNA regulatory networks, such as nuclear paraspeckle assembly transcript 1 (NEAT1)-miR-27b-3p-zinc finger E-box binding homeobox 1 (*Zeb1*) [7], taurine-upregulated gene 1 (TGU1)-miR-377-peroxisome proliferator-activated receptor gamma (*Pparg*) [2], cyclin-dependent kinase inhibitor 2B antisense RNA 1 (CDKN2B-AS1)--miR-15b-5p-wingless-Type family member 2B (*WNT2B*) [3] and potassium voltage-gated channel subfamily Q member 1 overlapping transcript 1 (KCNQ1OT1)-miR-147a-SRY-Box Transcription Factor 6 (*SOX6*) [8], have also been identified to play important roles in DN.

Typically, cytoplasmic lncRNAs can act as ceRNAs by sponging miRNAs, thereby regulating the expression levels of downstream target genes. Gm4419 is a newly identified proinflammatory lncRNA located on chromosome 12 (Chr12:21417911–21419803, 1730 bp). In a previous study, Yi et al. observed that Gm4419 is upregulated in HG-induced mesangial cells and mainly distributed in the cytoplasm of mesangial cells [9], suggesting that Gm4419 may function as a ceRNA and participate in the progression of DN. To validate this hypothesis, we predicted a potential DN-related lncRNA-miRNA-mRNA axis, namely Gm4419-miR-455-3p-histone deacetylase 2 (*Hdac2*), using bioinformatics methods in this study. Furthermore, we verified the role of this axis in DN using HG-treated mesangial cells. Our findings demonstrate that Gm4419 promotes mesangial cells proliferation and extracellular matrix accumulation by mediating the miR-455-3p/*Hdac2* axis.

2. Material and methods

2.1. Bioinformatics analysis

The keyword "Diabetic nephropathies" was retrieved to predict DN-related lncRNAs using the LncRNADisease v2.0 database (http://www.rnanut.net/lncrnadisease/index.php/home/search). The potential target miRNAs of Gm4419 were predicted using the miRDB database (http://www.mirdb.org/). Target genes of miR-455-3p were predicted using StarBase (http://starbase.sysu.edu.cn/), miRDB and TargetScan (http://www.targetscan.org/), followed by intersection using the jvenn tool (http://jvenn.toulouse.inra.fr/app/example.html). Gene interaction relationships were analyzed using the STRING database and visualized using the Network Analyzer tool of Cytoscape.

2.2. Cell authentication, culture and treatment

Mouse renal glomerular mesangial cells (SV40 MES-13 cells; #GNM21; RRID: CVCL_5368) were purchased from Shanghai Academy of Sciences (Shanghai, China) (https://www.cellbank.org.cn/search-detail.php?id=271). HEK 293 cells (RRID: CVCL_0045) were purchased from ATCC (Manassas, VA, USA). Prior to conducting *in vitro* experiments, DNA from SV40 MES-13 cells and HEK 293 cells were extracted and submitted for cell line authentication using a short tandem repeat (STR) profiling by Biowing Applied Biotechnology (Shanghai, China). The results of cell line authentication confirmed that the SV40 MES-13 cell line used in this study matched 100 % with an established SV40 MES-13 cell line. Additionally, the DNA profiling of the HEK 293 cell line was found to be match with the cell line in the cell line retrieval (the DSMZ database showed that the cells, called HEK 293, corresponded to the cell number CRL-1573). No multiple alleles were detected in either the SV40 MES-13 cell line or the HEK 293 cell line.

SV40 MES-13 mesangial cells were cultured in low-glucose DMEM medium (Sigma-Aldrich, St. Louis, MO, USA) supplemented with 10 % fetal bovine serum and 100 U/mL penicillin-streptomycin at 37 °C in a 5 % CO_2 incubator. To establish an *in vitro* DN cell model, mesangial cells were cultured under HG condition (by supplementing low-glucose DMEM medium with additional glucose to a final glucose concentration of 25 mmol/L) for 24 h (HG group). Mesangial cells in low-glucose condition (LG group: 5.5 mmol/L glucose) and mannitol condition (MA group: 5.5 mmol/L glucose + 19.5 mmol/L mannitol) were served as normal control and osmotic pressure control, respectively. HEK 293 cells were cultured in high-glucose DMEM medium (Sigma-Aldrich, St. Louis, MO, USA) with same condition as mesangial cells. Cultured cells were routinely checked by the PCR method to ensure that they are mycoplasma free.

2.3. Cell transfection

The following products were obtained from Genechem (Shanghai, China): negative control short hairpin RNA (shRNA) (sh-NC, 5′-CCTAAGGTTAAGTCGCCCTCG-3′), shRNA against Gm4419 (sh-Gm4419, 5′-AACCAAGCAGACCGAAGACT-3′) and *Hdac2* (sh-Hdac2, 5′-CAATGAGTTGCCATATAAT-3′), negative control mimic (NC mimic, 5′-UUCUCCGAACGUGUCACGU-3′), miR-455-3p mimic (miR mimic, 5′-CACAUAUACGGGCACCUGACG-3′), negative control inhibitor (inhibitor NC, 5′-CAGUACUUUUGUGUAGUACAA-3′), and miR-455-3p inhibitor (miR inhibitor, 5′- CGUCAGGUGCCCGUAUAUGUG-3′).

Cell transfection was performed using the following method. Briefly, mesangial cells (5×10^5 per well) were seeded into a 6-well

plate and allowed to grow until reaching 80–90 % confluence. 2 h prior to transfection, the DMEM medium was replaced with serum-free Opti-MEM medium (Invitrogen, Carlsbad, CA, USA). 5 μL transfection products (50 nM sh-Gm4419, 50 nM sh-Hdac2, 50 nM NC mimic, 50 nM miR-455-3p mimic, 100 nM NC inhibitor or 100 nM miR-455-3p inhibitor) and 5 μL Lipofectamine 2000 reagents (Thermo Fisher Scientific, Waltham, MA, USA) were separately dissolved in 250 μL Opti-MEM medium, gently mixed, placed at room temperature for 20 min and added into the cell-containing medium. 6 h post-transfection, the serum-free Opti-MEM medium was removed, and the cells were gently washed once with PBS. Subsequently, low-glucose DMEM medium supplemented with 10 % fetal bovine serum was used for cell culture. 48 h after transfection, cells were collected for subsequent experiments.

2.4. Reverse-transcription quantitative PCR (RT-qPCR)

Total RNA of mesangial cells was extracted using Trizol (Invitrogen, Carlsbad, CA, USA). Cytoplasmic and nuclear RNA were isolated using the PAKIS Kit (Thermo Fisher Scientific, Waltham, MA, USA). Complementary DNA was generated using either the miRNA Reverse Transcription Kit (Sangon, Shanghai, China) or the High-Capacity cDNA Reverse Transcription Kit (Thermo Fisher Scientific, Waltham, MA, USA). RT-qPCR was conducted on an ABI 7500 Real-Time PCR System (Applied Biosystems, Foster City, CA, USA). *U6* and glyceraldehyde-3-phosphate dehydrogenase (*Gapdh*) were used as control. The $2^{-\Delta\Delta C}$ method was adopted to calculate the relative expression of genes under the premise that the amplification efficiencies of target gene and internal reference gene are close to 100 %, and their difference is not more than 5 %. All primer sequences used in the present study are listed in Table 1.

2.5. Fluorescence in situ hybridization (FISH)

The Gm4419 FISH probe, labeled with Cy3, was synthesized with the following sequence: AGACCAA-CAGCATCTCTTCCCCATCCTGGTTGCAGGAGCTGGAACTTGAC by RiboBio (Guangzhou, China). FISH assay was performed according to the previous reported method [9]. Briefly, mesangial cells were collected after 24 h LG or HG treatment and fixed with 4 % paraformaldehyde for 10 min at room temperature. After pretreatment with pre-hybridization buffer at 37 °C for 30 min, cells were immersed in the hybridization solution containing Gm4419 FISH probe mix in a chamber at 37 °C overnight. Next, cells were stained with 6-diamidino-2-phenylindole (DAPI) (Beyotime Biotechnology, Jiangsu, China) after washing. Finally, images were captured using the NCF950 laser scanning confocal microscope (Zhejiang, China) under a 20× objective lens with a numerical aperture of 0.75.

2.6. RNA immunoprecipitation (RIP)

To assess whether Gm4419 was associated with RNA-induced silencing complex, an EZ-Magna RIP Kit (Millipore, Billerica, MA, USA) was used to perform the RIP assay. Briefly, cells were lysed with RIP lysis buffer and centrifuged to collect the supernatants. Cell supernatants were then incubated with protein A/G magnetic beads and Argonaute 2 (Ago2) (Abcam, Cambridge, MA, USA) or normal mouse IgG antibodies (Millipore, Billerica, MA, USA). RNA was extracted after nonspecific binding was removed with proteinase K buffer (Abcam, Cambridge, MA, USA). Finally, the expression levels of Gm4419 and miR-455-3p were determined by RT-qPCR.

2.7. Dual luciferase reporter assay

Wild-type sequences of Gm4419 (harboring binding sites for miR-455-3p) and mutant sequences of Gm4419 were amplified and inserted into the pmirGLO vector (Promega, Madison, WI, USA) to generate wild-type (Gm4419-WT) and mutant (Gm4419-MUT) reporter plasmids of Gm4419. Meanwhile, wild-type and mutant-type sequences of *Hdac2* 3′-untranslated region were also inserted into the pmirGLO vector to construct wild-type (Hdac2-WT) and mutant (Hdac2-MUT) reporter plasmids of *Hdac2*. To confirm the relationship between Gm4419 and miR-455-3p or miR-455-3p and *Hdac2*, dual luciferase reporter assay was performed. Briefly, HEK 293 cells (5×10^5 per well) were seeded into a 6-well plate and allowed to grow until reaching 80–90 % confluence. 2h prior to transfection, the DMEM medium was replaced with serum-free Opti-MEM medium. 5 μg Gm4419-WT/Gm4419-MUT/Hdac2-WT/Hdac2-MUT plasmid (or 5 μL NC mimic/miR-455-3p mimic) and 5 μL Lipofectamine 2000 reagents were separately dissolved in

Table 1
The primer sequences used in this study.

Name		Primer sequences
Gm4419	Forward primer	GGAACCAAGCAGACCGAAGAC
	Reverse primer	CCCCAACCCACAGGAACATAA
miR-455-3p	Forward primer	GAACTGCAGTCCATGGGCATA
	Reverse primer	GCAGGGTCCGAGGTATTC
Hdac2	Forward primer	ATACAACAGATCGCGTGATGAC
	Reverse primer	GGAACGTGAACTGCTTACCTT
Gapdh	Forward primer	ATCCCATCACCATCTTCC
	Reverse primer	GAGTCCTTCCACGATACCA
U6	Forward primer	GCTTCGGCAGCACATA
	Reverse primer	ATGGAACGCTTCACGA

Abbreviations: Hdac2, histone deacetylase 2; Gapdh, glyceraldehyde-3-phosphate dehydrogenase.

250 μL Opti-MEM medium, gently mixed, placed at room temperature for 20 min and added into the cell-containing medium. 6 h post-transfection, the serum-free Opti-MEM medium was removed, and the cells were gently washed once with PBS. Subsequently, high-glucose DMEM medium supplemented with 10 % fetal bovine serum was used for cell culture. RT-PCR method was used to evaluate the efficiency of transfection and efficiency>80 % was considered successful. 48 h after transfection, luciferase activity was measured using the Dual-Luciferase® Reporter assay system (Promega, Madison, WI, USA).

2.8. Cell counting kit-8 (CCK-8) assay and 5-ethynyl-2′-deoxyuridine (EdU) stainning

48 h after transfection, a CCK-8 Kit (Solarbio, Beijing, China) and an EdU labeling/detection Kit (RiboBio, Guangzhou, China) were adopted for cell proliferation detection. In the CCK-8 assay, 10 μL of CCK-8 solution was added into each well. 3 h later after incubation, the absorbance was measured at 450 nm using a microplate reader (Bio-Rad model 680; Bio-Rad, Hercules, CA, USA). In the EdU staining experiment, cells were placed in a 96-well plate and incubation with 50 μM of EdU for 2 h. Following fixation with 4 % paraformaldehyde and washing with phosphate-buffered saline and 0.5 % TritonX-100 in phosphate-buffered saline, cells were incubated with Apollo 567 working solution for 2 h. Finally, cells were counterstained with Hoechst 33342 for 30 min. EdU positive cells were observed using a fluorescence microscope (Olympus, Tokyo, Japan) and counted using Image J software (NIH Image, Bethesda, MD, USA).

2.9. Western blot analysis

The total protein of cultured cells was extracted using cold RIPA lysis buffer (Beyotime Biotechnology, Jiangsu, China). The protein concentration of cell lysates was detected using a BCA Protein Assay Kit (Beyotime Biotechnology, Jiangsu, China). Subsequently, protein lysates were separated with SDS-PAGE and electrophoretically transferred onto PVDF membranes. Following blocking with 5 % skimmed milk, the membranes were incubated with primary antibodies against collagen IV (Col-IV) (1:1000; Proteintech, Wuhan, China), fibronectin (FN) (1:1000; Proteintech), and transforming growth factor-beta 1 (TGF-β1) (1:500; Proteintech), and then with HRP-conjugated anti-mouse IgG (1:3000; CST, Beverly, MA, USA). Finally, the gel imaging analysis system (QMGENE, Beijing, China) and Image J software were used for analysis with GAPDH (1:5000; Abcam, Cambridge, MA, USA) as the internal reference.

2.10. Statistical analysis

Statistical analyses were done using SPSS 21.0 (IBM SPSS Inc., Chicago, IL, USA). Quantitative results were plotted as mean ± standard deviation (SD). Student's *t*-test or one-way analysis of variance with Tukey's post-hoc tests were used for data comparison, as appropriate. $P < 0.05$ was considered as statistically significant.

3. Results

3.1. The Gm4419-miR-455-3p-Hdac2 axis may be related with DN

10 causal DN-associated lncRNAs including Malat1 (Score: 0.9820, *Mus musculus*), 1700020I14Rik (Score: 0.9786, *Mus musculus*), MALAT1 (Score: 0.9630, *Homo sapiens*), PVT1 (Score: 0.9560, *Homo sapiens*), lnc-MGC (Score: 0.9462, *Homo sapiens*), Tmcc3 (Score: 0.9462, *Mus musculus*), NONRATT021972 (Score: 0.8808, *Homo sapiens*), Gm4419 (Score: 0.8808, *Mus musculus*), NONRATT021972 (Score: 0.8808, *Rattus norvegicus*), and CYP4B1-PS1 (Score: 0.5483, *Homo sapiens*) were found using the LncRNADisease v2.0 database.

Table 2
17 predicted target miRNAs for Gm4419.

Target Rank	Target Score	miRNA Name
1	89	mmu-miR-7214-3p
2	86	mmu-miR-351-3p
3	85	mmu-miR-455-3p
4	75	mmu-miR-6337
5	72	mmu-miR-2183
6	69	mmu-miR-7087-3p
7	68	mmu-miR-876-5p
8	60	mmu-miR-296-3p
9	59	mmu-miR-7038-5p
10	59	mmu-miR-6923-5p
11	57	mmu-miR-6992-5p
12	57	mmu-miR-434-3p
13	56	mmu-miR-20b-3p
14	56	mmu-miR-17-3p
15	56	mmu-miR-106a-3p
16	54	mmu-miR-7054-5p
17	54	mmu-miR-6999-5p

Among these causal lncRNAs, Gm4419 has received less attention in previous studies [9,10]; therefore, this lncRNA was focused on in this study.

Next, we predicted the target miRNAs of Gm4419. According to the miRDB database, there were a total of 17 candidate target miRNAs for Gm4419, among which mmu-miR-7214-3p, mmu-miR-351-3p, and mmu-miR-455-3p (hereafter called "miR-455-3p") had higher targeting relationship scores (Target Score >80) (Table 2). MiR-455-3p has been reported as an important regulator involved in the progression of DN [11,12]; therefore, this miRNA was chosen for subsequent analysis.

Using StarBase, miRDB and TargetScan, we predicted 1612, 393 and 292 candidate target genes of miR-455-3p, respectively (Supplementary Table 1). 74 overlapping candidate genes were identified using the jvenn tool (Fig. 1A). The interaction network of 74 overlapping genes was analyzed using the STRING database and visualized using Cytoscape (Fig. 1B). *Hdac2* was identified as the hub gene with the greatest level of interaction with other genes (Degree = 9).

Based on our bioinformatics analysis results, we speculated that the Gm4419-miR-455-3p-*Hdac2* axis may be associated with DN.

3.2. The Gm4419-miR-455-3p-Hdac2 axis is differently expressed in HG-treated mesangial cells

To explore the impact of HG-induced osmotic pressure on mesangial cells, mannitol was used as an osmotic pressure control. Our results showed that mannitol condition induced similar mesangial cells proliferation (Fig. 2A–C) and extracellular matrix accumulation (Fig. 2D) as LG condition; thus, the LG group was used as the control in subsequent experiments. As expected, an *in vitro* DN cell model was established under HG condition, characterized by obvious mesangial cells proliferation (Fig. 2A–C) and extracellular matrix accumulation as evidenced by the increased expressions of Col-IV, FN and TGF-β1 (Fig. 2D). The original images of Fig. 2D are provided in the Supplementary Fig. S1.

Next, our RT-qPCR results revealed that Gm4419 and *Hdac2* levels were increased and miR-455-3p was decreased in HG-treated mesangial cells as compared with LG-treated mesangial cells (Fig. 2E).

3.3. Gm4419 is mainly located in the cytoplasm of mesangial cells

It's well known that cytoplasmic lncRNA can act as an endogenous miRNA sponge to regulate the expression of downstream target genes. To explore the subcellular localization of Gm4419 in cells, the lncLocator (http://www.csbio.sjtu.edu.cn/bioinf/lncLocator/) was used and the data revealed that Gm4419 was mainly located in the cytoplasm (Fig. 3A). Next, our FISH (Fig. 3B) and RT-qPCR (Fig. 3C) results confirmed that Gm4419 was distributed in both the cytoplasm and nucleus but mainly in the cytoplasm of mesangial cells.

3.4. Gm4419 serves as a sponge of miR-455-3p

Based on the above-mentioned findings, we predicted that Gm4419 might serve as a sponge of miR-455-3p. To confirm this speculation, the binding sites of Gm4419 and miR-455-3p were predicted using the miRDB database (Fig. 4A). Next, RT-qPCR results

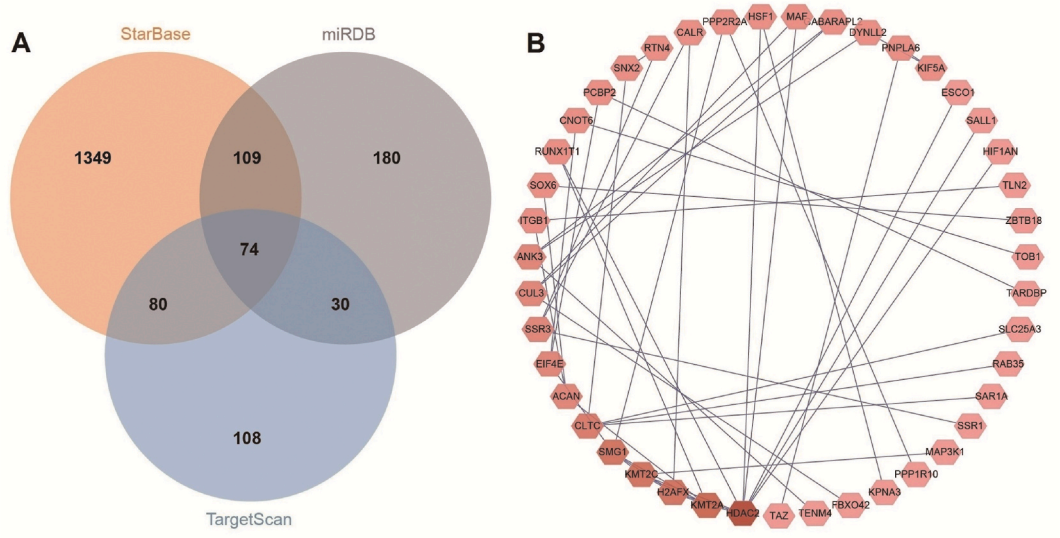

Fig. 1. The miR-455-3p-*Hdac2* axis is predicted by bioinformatics methods. (**A**): Target genes of miR-455-3p were intersected using the jvenn tool. 74 overlapping candidate genes were identified; (**B**): The interaction network of 74 candidate genes was analyzed using the STRING database and visualized using Cytoscape. *Hdac2* was identified as the hub gene with the greatest level of interaction with other genes. Hdac2, histone deacetylase 2.

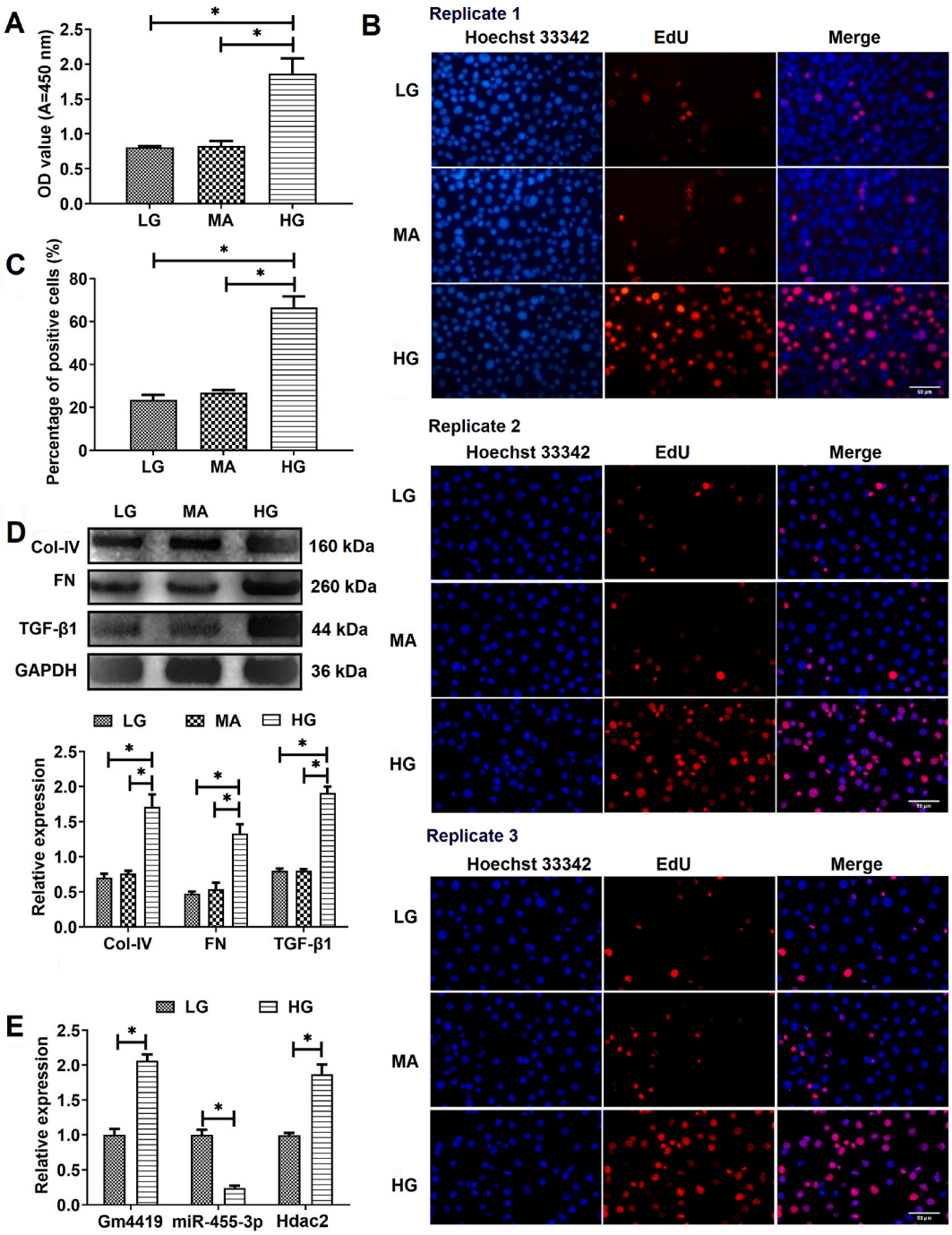

Fig. 2. Cell proliferation, extracellular matrix accumulation and expression of the Gm4419-miR-455-3p-*Hdac2* axis in HG-treated mesangial cells. CCK-8 assay (**A**) and EdU staining results (**B, C**) revealed significant mesangial cells proliferation in the HG group as compared with that in the LG group and the MA group. In EdU staining, nuclei were stained with Hoechst 33342. Blue (Hoechst 33342) indicated nuclei of total cells and Red (EdU) indicated nuclei of proliferating cells; scale bar = 50 μm; magnification = 200; (**D**): western blot results showed extracellular matrix accumulation in the HG group characterized by the increased expressions of Col-IV, FN and TGF-β1; (**E**): RT-qPCR showed Gm4419 and *Hdac2* levels were increased and miR-455-3p was decreased in the HG group as compared with that in the LG group. In RT-qPCR experiment, *U6* was used to normalize the expression level of miR-455-3p and *Gapdh* was used for Gm4419 and *Hdac2*. Data are presented as mean ± SD. One-way analysis of variance with Tukey's post-hoc tests was used for data comparison. $N = 3$; $^*p < 0.05$. CCK-8, cell counting kit-8; EdU, 5-ethynyl-2′-deoxyuridine; LG, low glucose; MA, mannitol; HG, high glucose; Col- IV, collagen IV; FN, fibronectin; TGF-β1, transforming growth factor-beta 1; Hdac2, histone deacetylase 2; RT-qPCR, reverse-transcription quantitative PCR; Gapdh, glyceraldehyde-3-phosphate dehydrogenase.

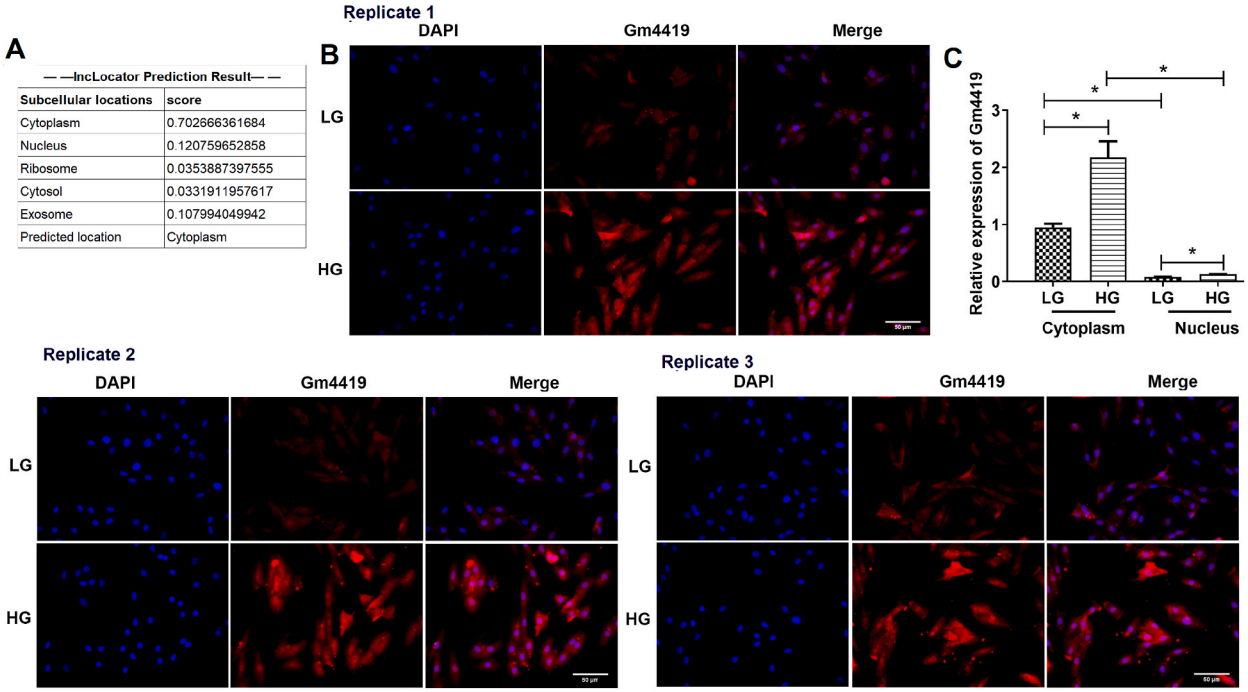

Fig. 3. Gm4419 is mainly distributed in the cytoplasm of mesangial cells. (**A**): lncLocator prediction result; FISH (**B**) and RT-qPCR (**C**) results confirmed that Gm4419 was distributed in both the cytoplasm and nucleus but mainly in the cytoplasm of mesangial cells. In FISH experiment, nuclei were stained with DAPI; scale bar = 50 μm; magnification = 200. In RT-qPCR experiment, *Gapdh* was used to normalize the expression level of Gm4419. Data are presented as mean ± SD. Student's *t*-test was used for data comparison. $N = 3$; $^*p < 0.05$. LG, low glucose; HG, high glucose; FISH, Fluorescence in situ hybridization; RT-qPCR, reverse-transcription quantitative PCR; DAPI, 6-diamidino-2-phenylindole; Gapdh, glyceraldehyde-3-phosphate dehydrogenase.

revealed that the expression of miR-455-3p in the sh-Gm4419 transfected cells was significantly increased as compared with that of the sh-NC transfected cells (Fig. 4B).

To further validate the interaction between Gm4419 and miR-455-3p, miR-455-3p mimic was transfected to up-regulate the expression of miR-455-3p in HG-treated mesangial cells (Fig. 4C). Subsequently, the dual luciferase reporter assay results showed that the miR-455-3p mimic significantly reduced the luciferase activity in cells containing the Gm4419-WT reporter but had no effect in cells containing the Gm4419-MUT reporter (Fig. 4D). Moreover, RIP results revealed higher levels of Gm4419 and miR-455-3p in the Ago2 RIP group than those in the IgG control group (Fig. 4E). Collectively, our results suggest that Gm4419 serves as a sponge of miR-455-3p.

3.5. *Hdac2 is a target of miR-455-3p*

The binding sites of miR-455-3p and *Hdac2* were obtained through StarBase (Fig. 5A). Next, our RT-qPCR results revealed that miR-455-3p mimic transfection increased the expression of miR-455-3p but decreased *Hdac2* expression (Fig. 5B). Moreover, our dual luciferase reporter assay revealed that the miR-455-3p mimic significantly reduced the luciferase activity in cells containing the Hdac2-WT reporter but had no effect in cells containing the Hdac2-MUT reporter (Fig. 5C).

3.6. *Gene silencing of Gm4419 inhibits mesangial cells proliferation and extracellular matrix accumulation by mediating the miR-455-3p/Hdac2 axis*

To explore the role of the Gm4419/miR-455-3p/*Hdac2* axis on mesangial cells proliferation and extracellular matrix accumulation, HG-treated mesangial cells were subjected to shRNA and/or inhibitor interventions. Our RT-qPCR results revealed that sh-Gm4419 treatment reduced the expressions of Gm4419 and *Hdac2* but increased the expression of miR-455-3p; while, the expression levels of miR-455-3p and *Hdac2* were reversed upon the addition of a miR-455-3p inhibitor. Furthermore, the impact of the miR-455-3p inhibitor on *Hdac2* expression was counteracted by sh-Hdac2 treatment (Fig. 6A). The CCK-8 assay results depicted that sh-Gm4419 treatment resulted in suppressed cell proliferation, while the miR-455-3p inhibitor counteracted the suppression effect of sh-Gm4419, which was reversed again by adding sh-Hdac2 (Fig. 6B). Consistent findings were observed in the EdU staining (Fig. 6C and D), as well as in the western blot analysis of Col-IV, FN, and TGF-β1 (Fig. 6E). The original images of Fig. 6E are provided in the Supplementary Fig. S2.

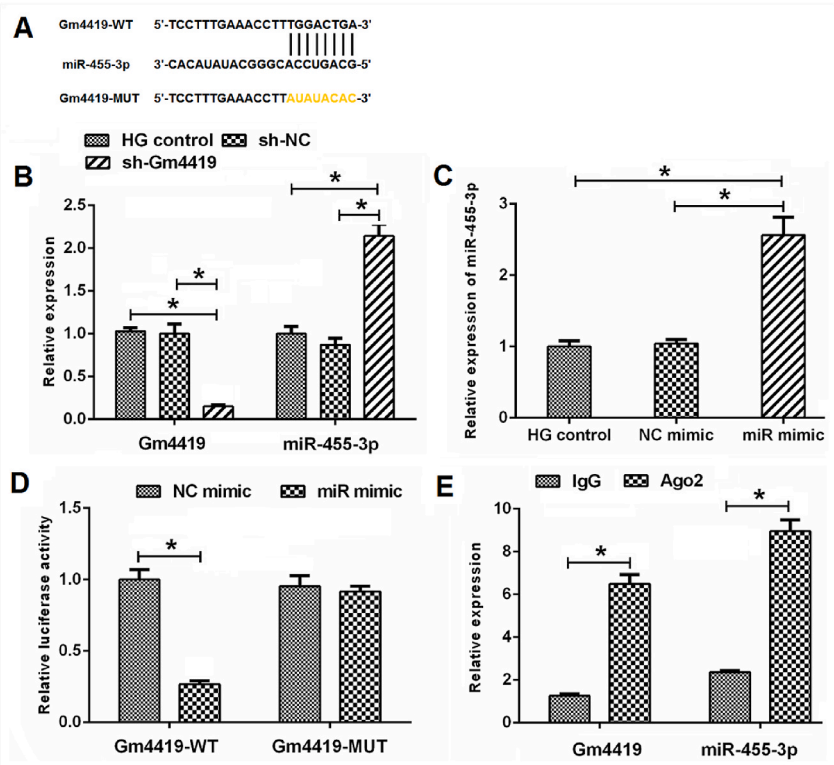

Fig. 4. The interaction between Gm4419 and miR-455-3p. (**A**): miRDB database predicted the binding sites between Gm4419 and miR-455-3p; (**B**) RT-qPCR results revealed that Gm4419 was decreased and miR-455-3p was increased after sh-Gm4419 transfection in HG-treated mesangial cells; (**C**): RT-qPCR results revealed that miR-455-3p was increased after miR-455-3p mimic transfection in HG-treated mesangial cells; (**D**): Dual luciferase reporter assay was performed in HEK 293 cells co-transfected with Gm4419-WT or Gm4419-MUT and miR-455-3p mimic or NC mimic; (**E**): RIP assay suggested that higher levels of Gm4419 and miR-455-3p were enriched in the Ago2 RIP group than those in the IgG control group. In RT-qPCR experiment, *Gapdh* was used to normalize the expression level of Gm4419 and *U6* was used for miR-455-3p. Data are presented as mean ± SD. One-way analysis of variance with Tukey's post-hoc tests was used for data comparison. $N = 3$; $^*p < 0.05$. HG, high glucose; NC mimic, negative control mimic; miR mimic, miR-455-3p mimic; Gm4419-WT, wild-type reporter plasmid of Gm4419; Gm4419-MUT, mutant-type reporter plasmid of Gm4419; RIP, RNA immunoprecipitation; RT-qPCR, reverse-transcription quantitative PCR; Gapdh, glyceraldehyde-3-phosphate dehydrogenase.

4. Discussion

Mesangial cells proliferation and extracellular matrix accumulation are the main pathological characteristics of DN. Therapeutic strategies that improve these characteristics may be beneficial for the treatment and control of this disease. In the present study, we identified a potential DN-related axis, Gm4419-miR-455-3p-*Hdac2*, through bioinformatics analysis. We found that Gm4419 was highly expressed in HG-treated mesangial cells and Gm4419 gene silencing could inhibit mesangial cells proliferation and extracellular matrix accumulation by mediating the miR-455-3p/*Hdac2* axis.

Gm4419 is a relatively new lncRNA that has not been extensively studied, especially in relation to DN. In a previous study reported by Yi et al., authors found that Gm4419 expression is significantly increased in HG-treated mesangial cells and Gm4419 gene silencing relieves nuclear factor kappa B (NF-κB)/NACHT, LRR and PYD domain-containing protein 3 (NLRP3) inflammasome-mediated inflammations in DN [9]. Additionally, Li et al. demonstrated that Gm4419 mitigates kidney injury in DN rats through the NF-κB pathway [10]. In this study, we found that Gm4419 was elevated in HG-treated mesangial cells and Gm4419 gene silencing significantly inhibited HG-induced mesangial cells proliferation and extracellular matrix accumulation. These findings suggest that Gm4419 may be a potential therapeutic target for DN.

The subcellular localization of lncRNAs greatly influences their roles. According to the ceRNA hypothesis, whether a lncRNA functions as an effective ceRNA primarily depends on its abundance and subcellular localization in the cytoplasm [13]. In our study, we found that Gm4419 was predominantly distributed in the cytoplasm of mesangial cells, which is consistent with previous observations [9]. To our knowledge, no previous studies have explored the potential role of Gm4419 as a ceRNA in DN. Thus, in this study, we predicted and verified the Gm4419-miR-455-3p-*Hdac2* ceRNA network, which represents the first reported Gm4419-related ceRNA network in DN.

miRNAs play important roles in the pathogenesis of DN [14]. As a well-characterized miRNA, miR-455-3p has been demonstrated to be involved in many diseases such as cancers [15–18] and Alzheimer's disease [19–22]. In this study, we focused on miR-455-3p for two main reasons. Firstly, the miRDB database indicated a potential binding between Gm4419 and miR-455-3p, and their interaction

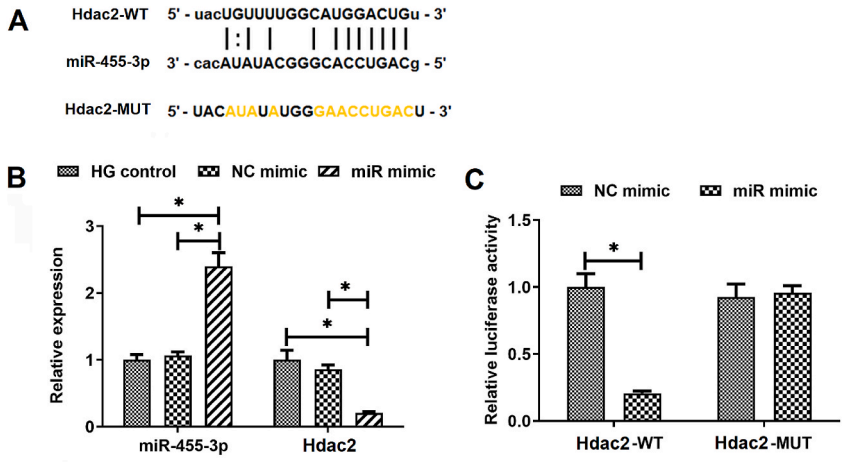

Fig. 5. *Hdac2* is a target gene of miR-455-3p. (**A**): StarBase predicted the binding sites of miR-455-3p and *Hdac2*; (**B**): miR-455-3p mimic was used to increase the expression of miR-455-3p and decrease the expression of *Hdac2* in HG-treated mesangial cells. *Gapdh* was used to normalize the expression level of *Hdac2* and *U6* was used for miR-455-3p; (**C**): Dual luciferase reporter assay was performed in HEK 293 cells to confirm the target association between miR-455-3p and *Hdac2*. Data are presented as mean ± SD. One-way analysis of variance with Tukey's post-hoc tests was used for data comparison. $N = 3$; $^*p < 0.05$. HG, high glucose; NC mimic, negative control mimic; miR mimic, miR-455-3p mimic; Hdac2-WT, wild-type reporter plasmid of *Hdac2*; Hdac2-MUT, mutant-type reporter plasmid of *Hdac2*; Hdac2, histone deacetylase 2.

has been demonstrated in a hepatic ischemia/reperfusion injury study [23]. Secondly, recent studies have shown a protective role of miR-455-3p in DN. For instance, Wu et al. reported that miR-455-3p is down-regulated in HG-treated human mesangial cells and miR-455-3p overexpression improves renal fibrosis by targeting rho-associated coiled-coil-containing protein kinase 2 (*ROCK2*) [11]. Wang et al. demonstrated that miR-455-3p plays a protective role on HG-induced apoptosis, inflammation, oxidative stress, and fibrogenesis in mouse mesangial cells by targeting highmobility group box 1 (*Hmgb1*) [12]. Our results showed that miR-455-3p was down-regulated in HG-treated mesangial cells, consistent with previous studies [11,12,24]. Additionally, we verified the interaction between Gm4419 and miR-455-3p through dual luciferase reporter assay, and found miR-455-3p inhibitor reversed the impact of Gm4419 gene silencing on mesangial cells proliferation and extracellular matrix accumulation. Together, these results suggest that Gm4419 exerts its function in HG-treated mesangial cells by sponging miR-455-3p.

As a member of the class I HDAC enzymes, HDAC2 has been closely associated with diabetes-related disorders, including DN. For instance, Noh et al. found that HDAC2 activity is increased in *in-vivo* and *in-vitro* diabetic renal fibrosis models, and HDAC inhibitors protects against renal fibrosis induced by diabetes or TGF-β1 [25]. Du et al. demonstrated that sodium butyrate mitigates renal damage in diabetic *db/db* mice and inhibits HG-induced apoptosis in NRK-52E cells through inhibiting HDAC2 [26]. Elevated expression of HDAC2 was also observed in renal tissues of diabetic rats, mice, and patients [27]. Consistent with these findings, our study revealed high level of HDAC2 in HG-induced mesangial cells. The target association between miR-455-3p and HDAC2 has been widely reported [28–32]. In this study, we also confirmed this interaction in HEK 293 cells using a dual luciferase reporter assay, which was further supported by the fact that *Hdac2* gene silencing could reverse the impact of miR-455-3p inhibitor on mesangial cells proliferation and extracellular matrix accumulation.

5. Conclusion

Gene silencing of Gm4419 inhibits HG-induced mesangial cells proliferation and extracellular matrix accumulation by regulating the miR-455-3p/*Hdac2* axis, suggesting the Gm4419-miR-455-3p-*Hdac2* axis may serve as a potential therapeutic target for diabetic nephropathy treatment. In future, more experiments are required to validate the role of this axis *in vivo* and assess its potential clinical applications.

Disclosure statement

The authors have no relevant financial or non-financial interests to disclose.

Funding

This work was supported by research grant from of Chongqing Health Commission (2022WSJK012).

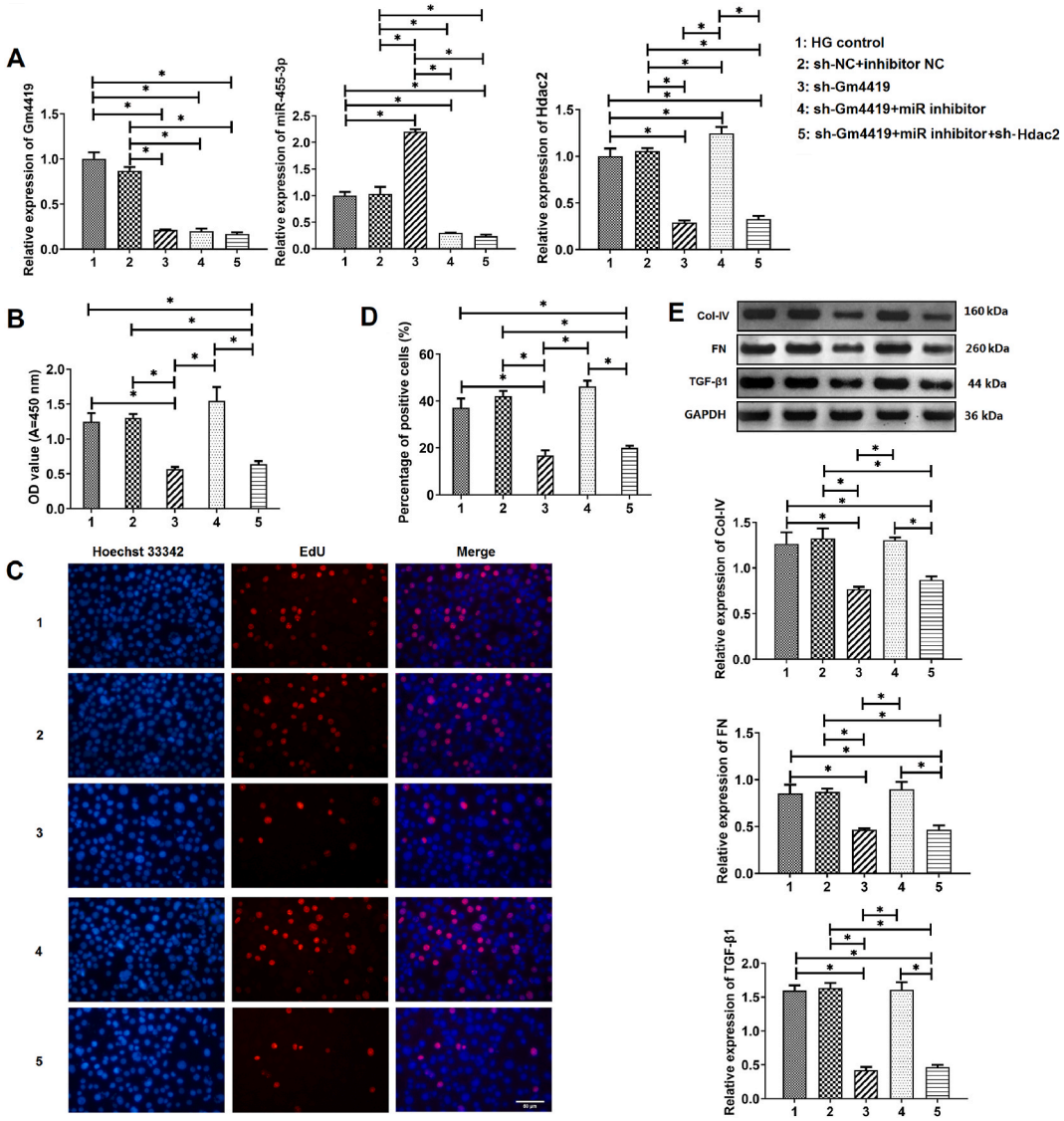

Fig. 6. Gene silencing of Gm4419 inhibits mesangial cells proliferation and extracellular matrix accumulation by mediating the miR-455-3p/*Hdac2* axis in HG-treated mesangial cells. (**A**): RT-qPCR results of Gm4419, miR-455-3p and *Hdac2* in HG-induced mesangial cells treated with sh-Gm4419, miR-455-3p inhibitor and/or sh-Hdac2. *Gapdh* was used to normalize the expression levels of Gm4419 and *Hdac2* and *U6* was used to for miR-455-3p; CCK-8 assay (**B**) and EdU staining (**C, D**) results of cell proliferation in HG-induced mesangial cells treated with sh-Gm4419, miR-455-3p inhibitor and/or sh-Hdac2. In EdU staining, nuclei were stained with Hoechst 33342. Blue (Hoechst 33342) indicated nuclei of total cells and Red (EdU) indicated nuclei of proliferating cells; scale bar = 50 μm; magnification = 200; (**E**): western blot results of Col-IV, FN and TGF-β1 in HG-induced mesangial cells treated with sh-Gm4419, miR-455-3p inhibitor and/or sh-Hdac2. Data are presented as mean ± SD. One-way analysis of variance with Tukey's post-hoc tests was used for data comparison. $N = 3$; *$p < 0.05$. CCK-8, cell counting kit-8; EdU, 5-ethynyl-2′-deoxyuridine; RT-qPCR, reverse-transcription quantitative PCR; GAPDH, glyceraldehyde-3-phosphate dehydrogenase; HG, high glucose; Col- IV, collagen IV; FN, fibronectin; TGF-β1, transforming growth factor-beta 1; Hdac2, histone deacetylase 2; miR inhibitor, miR-455-3p inhibitor.

Data availability statement

All data used in the generation of the results presented in this manuscript will be made available upon reasonable request from the corresponding author.

CRediT authorship contribution statement

Yang Wen: Writing – original draft, Methodology, Investigation, Formal analysis, Data curation. **Hua Gan:** Investigation, Formal analysis, Data curation. **Qing Zhong:** Investigation, Formal analysis, Data curation. **Ying Gong:** Writing – review & editing,

Investigation, Funding acquisition, Formal analysis, Data curation, Conceptualization.

Declaration of competing interest

The authors declare that they have no known competing financial interests or personal relationships that could have appeared to influence the work reported in this paper.

Acknowledgement

We would like to thank Editage (www.editage.cn) for English language editing.

List of abbreviations

CCK-8	Cell counting kit-8
Col-IV	collagen IV
ceRNAs	competitive endogenous RNAs
shRNA	short hairpin RNA
DN	Diabetic nephropathy
EdU	5-ethynyl-2′-deoxyuridine
FN	fibronectin
FISH	Fluorescence in situ hybridization
GAPDH	glyceraldehyde-3-phosphate dehydrogenase
Hdac2	histone deacetylase 2
HG	High glucose
LncRNAs	long noncoding RNAs
LG	low glucose
MA	mannitol
MiRNAs	microRNAs
RT-qPCR	Reverse-transcription quantitative PCR
RIP	RNA immunoprecipitation
SD	standard deviation
TGF-β1	transforming growth factor-beta 1

Appendix A. Supplementary data

Supplementary data to this article can be found online at https://doi.org/10.1016/j.heliyon.2024.e38835.

References

[1] C.W. Tung, Y.C. Hsu, Y.H. Shih, P.J. Chang, C.L. Lin, Glomerular mesangial cell and podocyte injuries in diabetic nephropathy, Nephrology 23 (s4) (2018) 32–37, https://doi.org/10.1111/nep.13451.
[2] L.J. Duan, M. Ding, L.J. Hou, Y.T. Cui, C.J. Li, D.M. Yu, Long noncoding RNA TUG1 alleviates extracellular matrix accumulation via mediating microRNA-377 targeting of PPARγ in diabetic nephropathy, Biochem. Biophys. Res. Commun. 484 (3) (2017) 598–604, https://doi.org/10.1016/j.bbrc.2017.01.145.
[3] J. Chang, Y. Yu, Z. Fang, H. He, D. Wang, J. Teng, et al., Long non-coding RNA CDKN2B-AS1 regulates high glucose-induced human mesangial cell injury via regulating the miR-15b-5p/WNT2B axis, Diabetol. Metab. Syndr. 12 (1) (2020) 109, https://doi.org/10.1186/s13098-020-00618-z.
[4] J. Li, M. Li, L. Bai, KCNQ1OT1/miR-18b/HMGA2 axis regulates high glucose-induced proliferation, oxidative stress, and extracellular matrix accumulation in mesangial cells, Mol. Cell. Biochem. 476 (1) (2021) 321–331, https://doi.org/10.1007/s11010-020-03909-1.
[5] J. Lv, Y. Wu, Y. Mai, S. Bu, Noncoding RNAs in diabetic nephropathy: pathogenesis, biomarkers, and therapy, J. Diabetes Res. 2020 (2020) 3960857, https://doi.org/10.1155/2020/3960857.
[6] X.L. Zhang, H.Q. Zhu, Y. Zhang, C.Y. Zhang, J.S. Jiao, X.Y. Xing, LncRNA CASC2 regulates high glucose-induced proliferation, extracellular matrix accumulation and oxidative stress of human mesangial cells via miR-133b/FOXP1 axis, Eur. Rev. Med. Pharmacol. Sci. 24 (2) (2020) 802–812, https://doi.org/10.26355/eurrev_202001_20063.
[7] X. Wang, Y. Xu, Y.C. Zhu, Y.K. Wang, J. Li, X.Y. Li, et al., LncRNA NEAT1 promotes extracellular matrix accumulation and epithelial-to-mesenchymal transition by targeting miR-27b-3p and ZEB1 in diabetic nephropathy, J. Cell. Physiol. 234 (8) (2019) 12926–12933, https://doi.org/10.1002/jcp.27959.
[8] Y. Xu, X. Zhan, lncRNA KCNQ1OT1 regulated high glucose-induced proliferation, oxidative stress, extracellular matrix accumulation, and inflammation by miR-147a/SOX6 in diabetic nephropathy (DN), Endocr. J. 69 (5) (2022) 511–522, https://doi.org/10.1507/endocrj.EJ21-0514.
[9] H. Yi, R. Peng, L.Y. Zhang, Y. Sun, H.M. Peng, H.D. Liu, et al., LincRNA-Gm4419 knockdown ameliorates NF-κB/NLRP3 inflammasome-mediated inflammation in diabetic nephropathy, Cell Death Dis. 8 (2) (2017) e2583, https://doi.org/10.1038/cddis.2016.451.
[10] H. Li, P. Wu, D. Sun, L. Jiang, J. Yu, C. Wang, et al., LncRNA-Gm4419 alleviates renal damage in rats with diabetic nephropathy through NF-κB pathway, Panminerva, Med. 65 (2) (2023) 268–269, https://doi.org/10.23736/S0031-0808.19.03844-8.
[11] J. Wu, J. Liu, Y. Ding, M. Zhu, K. Lu, J. Zhou, et al., MiR-455-3p suppresses renal fibrosis through repression of ROCK2 expression in diabetic nephropathy, Biochem. Biophys. Res. Commun. 503 (2) (2018) 977–983, j.bbrc.2018.06.105.
[12] J. Wang, S. Yang, W. Li, M. Zhao, K. Li, Circ_0000491 promotes apoptosis, inflammation, oxidative stress, and fibrosis in high glucose-induced mesangial cells by regulating miR-455-3p/hmgb1 Axis, Nephron 146 (1) (2022) 72–83, https://doi.org/10.1159/000516870.

[13] T. Zhang, C. Chen, S. Han, L. Chen, H. Ding, Y. Lin, Integrated analysis reveals a lncRNA-miRNA-mRNA network associated with pigeon skeletal muscle development, Genes 12 (11) (2021) 1787, https://doi.org/10.3390/genes12111787.
[14] H. Zhou, W.J. Ni, X.M. Meng, L.Q. Tang, MicroRNAs as regulators of immune and inflammatory responses: potential therapeutic targets in diabetic nephropathy, Front. Cell Dev. Biol. 8 (2020) 618536, https://doi.org/10.3389/fcell.2020.618536.
[15] X. Gao, H. Zhao, C. Diao, X. Wang, Y. Xie, Y. Liu, et al., miR-455-3p serves as prognostic factor and regulates the proliferation and migration of non-small cell lung cancer through targeting HOXB5, Biochem. Biophys. Res. Commun. 495 (1) (2018) 1074–1080, https://doi.org/10.1016/j.bbrc.2017.11.123.
[16] L. Chai, X.J. Kang, Z.Z. Sun, M.F. Zeng, S.R. Yu, Y. Ding, et al., MiR-497-5p, miR-195-5p and miR-455-3p function as tumor suppressors by targeting hTERT in melanoma A375 cells, Cancer Manag. Res. 10 (2018) 989–1003, https://doi.org/10.2147/CMAR.S163335.
[17] T. Zhan, Q. Zhu, Z. Han, J. Tan, M. Liu, W. Liu, et al., miR-455-3p functions as a tumor suppressor by restraining wnt/β-catenin signaling via TAZ in pancreatic cancer, Cancer Manag. Res. 12 (2020) 1483–1492, https://doi.org/10.2147/CMAR.S235794.
[18] T. Zhan, M. Chen, W. Liu, Z. Han, Q. Zhu, M. Liu, et al., MiR-455-3p inhibits gastric cancer progression by repressing Wnt/β-catenin signaling through binding to ARMC8, BMC. Med. Genomics. 16 (1) (2023) 155, https://doi.org/10.1186/s12920-023-01583-y.
[19] S. Kumar, M. Vijayan, P.H. Reddy, MicroRNA-455-3p as a potential peripheral biomarker for Alzheimer's disease, Hum. Mol. Genet. 26 (19) (2017) 3808–3822, https://doi.org/10.1093/hmg/ddx267.
[20] S. Kumar, A.P. Reddy, X. Yin, P.H. Reddy, Novel MicroRNA-455-3p and its protective effects against abnormal APP processing and amyloid beta toxicity in Alzheimer's disease, Biochim. Biophys. Acta, Mol. Basis Dis. 1865 (9) (2019) 2428–2440, https://doi.org/10.1016/j.bbadis.2019.06.006.
[21] S. Kumar, P.H. Reddy, A new discovery of MicroRNA-455-3p in alzheimer's disease, J. Alzheimers. Dis. 72 (s1) (2019) S117, https://doi.org/10.3233/JAD-190583, s30.
[22] S. Kumar, H. Morton, N. Sawant, E. Orlov, L.E. Bunquin, J.A. Pradeepkiran, et al., MicroRNA-455-3p improves synaptic, cognitive functions and extends lifespan: relevance to Alzheimer's disease, Redox, Biol. 48 (2021) 102182, https://doi.org/10.1016/j.redox.2021.102182.
[23] D. Ying, X. Zhou, Y. Ruan, L. Wang, X. Wu, LncRNA Gm4419 induces cell apoptosis in hepatic ischemia-reperfusion injury via regulating the miR-455-SOX6 axis, Biochem. Cell. Biol. 98 (4) (2020) 474–483, https://doi.org/10.1139/bcb-2019-0331.
[24] X.J. Zhu, Z. Gong, S.J. Li, H.P. Jia, D.L. Li, Long non-coding RNA Hottip modulates high-glucose-induced inflammation and ECM accumulation through miR-455-3p/WNT2B in mouse mesangial cells, Int. J. Clin. Exp. Pathol. 12 (7) (2019) 2435–2445.
[25] H. Noh, E.Y. Oh, J.Y. Seo, M.R. Yu, Y.O. Kim, H. Ha, et al., Histone deacetylase-2 is a key regulator of diabetes- and transforming growth factor-beta1-induced renal injury, Am. J. Physiol. Renal. Physiol. 297 (3) (2009) F729–F739, https://doi.org/10.1152/ajprenal.00086.2009.
[26] Y. Du, G. Tang, W. Yuan, Suppression of HDAC2 by sodium butyrate alleviates apoptosis of kidney cells in db/db mice and HG-induced NRK-52E cells, Int. J. Mol. Med. 45 (1) (2020) 210–222, https://doi.org/10.3892/ijmm.2019.4397.
[27] X. Wang, J. Liu, J. Zhen, C. Zhang, Q. Wan, G. Liu, et al., Histone deacetylase 4 selectively contributes to podocyte injury in diabetic nephropathy, Kidney, Int 86 (4) (2014) 712–725, https://doi.org/10.1038/ki.2014.111.
[28] S. Guo, Y. Zhen, Z. Zhu, G. Zhou, X. Zheng, Cinnamic acid rescues behavioral deficits in a mouse model of traumatic brain injury by targeting miR-455-3p/HDAC2, Life Sci. 235 (2019) 116819, https://doi.org/10.1016/j.lfs.2019.116819.
[29] H. You, L. Wang, F. Bu, H. Meng, X. Pan, J. Li, et al., The miR-455-3p/HDAC2 axis plays a pivotal role in the progression and reversal of liver fibrosis and is regulated by epigenetics, FASEB. J. 35 (7) (2021) e21700, https://doi.org/10.1096/fj.202002319RRR.
[30] N. Li, X.J. Chen, Y.H. Zeng, L.P. Zeng, K. Hu, L.J. Chen, Silencing of lncRNA CRNDE attenuates nonsmall-cell lung cancer progression by mediating the miR-455-3p/HDAC2 axis, Kaohsiung, J. Med. Sci. 38 (8) (2022) 749–760, https://doi.org/10.1002/kjm2.12558.
[31] F. Ma, J. Huang, W. Li, P. Li, M. Liu, H. Xue, MicroRNA-455-3p functions as a tumor suppressor by targeting HDAC2 to regulate cell cycle in hepatocellular carcinoma, Environ. Toxicol. 37 (7) (2022) 1675–1685, https://doi.org/10.1002/tox.23516.
[32] H. Ma, M. Li, Z. Jia, X. Chen, N. Bu, MicroRNA-455–3p promotes osteoblast differentiation via targeting HDAC2, Injury 53 (11) (2022) 3636–3641, https://doi.org/10.1016/j.injury.2022.08.047.